Journal of Solid State Chemistry 183 (2010) 662–667

Contents lists available at ScienceDirect

Journal of Solid State Chemistry

journal homepage: www.elsevier.com/locate/jssc

Kirkendall-effect-based growth of dendrite-shaped CuO hollow micro/nanostructures for lithium-ion battery anodes

Yingying Hu *, Xintang Huang *, Kai Wang, Jinping Liu, Jian Jiang, Ruimin Ding, Xiaoxu Ji, Xin Li

Center for Nanoscience and Nanotechnology, Huazhong Normal University, Wuhan 430079, Hubei, PR China

ARTICLE INFO

Article history:
Received 5 October 2009
Received in revised form
13 January 2010
Accepted 14 January 2010
Available online 20 January 2010

Keywords:
Kirkendall effect
3D CuO nanostructure
Hollow structure
Li-ion battery

ABSTRACT

Three-dimensional (3D) dendrite-shaped CuO hollow micro/nanostructures have been prepared *via* a Kirkendall-effect-based approach for the first time and have been demonstrated as a high-performance anode material for lithium-ion batteries. The as-prepared hollow structures were investigated by scanning electron microscopy, transmission electron microscopy, X-ray diffraction, and electrochemical properties. A CuO hollow structure composed of nanocubes outside and a dense film inside was selected as a typical example of the optimized design; it exhibited significantly improved cyclability at a current rate of 0.5 C, with the average Coulombic efficiency of ~97.0% and 57.9% retention of the discharge capacity of the second cycle after 50 cycles. The correlation between the structure features of the hollow CuO and their electrochemical behavior was discussed in detail. Smaller size of primary structure and larger internal space of electrode materials are crucial to better electrochemical performance. This work represents that Kirkendall effect is a promising method to fabricate excellent hollow electrode materials for Li-ion batteries.

1. Introduction

Due to their high surface area, low material density, and surface permeability [1], hollow structures with nanometer to micrometer dimensions have emerged as intriguing architectures for applications in catalysis, drug delivery, nanoelectronics, and sensor systems [1–4]. With regard to metal and metal oxides hollow structures, palladium nanotube, Co_3O_4 hollow microspheres, and copper oxide hollow microfibers have also been synthesized by various methods, including template-sacrificial strategies, nanoscale acid etching, and Kirkendall effect [5–7]. Among them, the merits of the Kirkendall-effect-based method are obvious, that is, it is template-free and needs no layered materials, while being capable of producing both binary and ternary and even more complicated systems [8].

Copper oxide with nanometer-scale dimension and morphological specificity is an advanced material with potential for diverse applications [9–11]. Over the past years, many efforts have been directed toward the fabrication of nanostructured CuO to improve its performance in currently existing applications. Among these CuO nanostructures, 1D nanomaterials have been largely prepared through various routes [12–14]. However, synthesizing 2D and 3D structures of CuO nanomaterials has been an active research field [15,16]. Up to now, very few publications on the fabrication of 2D and 3D CuO hollow structures without the assistance of templates has been reported [17]. In recent years, CuO among transition-metal oxides, which have become promising candidates for anode materials of Li-ion batteries due to their huge specific capacity [18,19], is of particular interest for its inexpensiveness and nontoxicity. The electrochemical process of the CuO electrode is expected to evolve the following reaction:

$$CuO + 2Li^+ + 2e^- \leftrightarrow Cu + Li_2O$$

with a total associated capacity of 670 mA h g^{-1} based on a maximum uptake of 2 Li per CuO [20]. Many efforts toward enabling CuO and CuO-based composites with diverse morphologies to improve the electrochemical capability of Li-ion batteries should be demonstrated (see Table S1 in the Supporting Information) [17,21–25].

Herein, novel dendrite-shaped CuO hollow micro/nanostructures have been successfully fabricated through a template-free Kirkendall-effect-based approach from dendritic Cu precursors prepared simply at room temperature. A CuO hollow microstructure composed of nanocubes outside and a dense film inside was selected as a typical example of the optimized design; it exhibited enhanced cyclability at a current rate of 0.5 C as a anode material for lithium-ion battery, with the average Coulombic efficiency of ~97.0% and 57.9% retention of the discharge capacity of the second cycle after 50 cycles. To the best of our knowledge, this is the first

* Corresponding authors. Fax: +86 027 67861185.
E-mail addresses: yyhu@phy.ccnu.edu.cn (Y. Hu), xthuang@phy.ccnu.edu.cn (X. Huang).

0022-4596/$ - see front matter © 2010 Elsevier Inc. All rights reserved.
doi:10.1016/j.jssc.2010.01.013

time to investigate the electrochemical reaction of lithium with hollow active materials synthesized through Kirkendall effect, which is confirmed to be a promising method to prepare excellent hollow electrode materials for Li-ion batteries.

2. Experimental section

Dendrite-shaped CuO hollow structures composed of nanocubes were synthesized by a two-step method using the copper chloride dihydrate ($CuCl_2 \cdot 2H_2O$), acetic acid (HAc; CH_3COOH) and aluminum (Al) foils, all purchased from Shanghai Chemical Reagent Co., Ltd. Prior to the synthesis, Al foils were carefully cleaned with absolute alcohol and distilled water, respectively, for several times. In the first step, 1.02 g of $CuCl_2 \cdot 2H_2O$ was dissolved in 200 mL distilled water, and magnetically stirred to become settled. Two milliliters acetic acid was added into the previous aqueous solution drop by drop under stirring. The cleaned Al foil was then immersed into the beaker with the as-prepared mixture solution for 4 h at room temperature. After reaction, Al foil and the reaction solution were removed and the red precursors formed loosely on the surface of Al foil were filtered and rinsed thoroughly with distilled water, then dried in vacuum drying oven at ambient temperature for further reaction. In the second step, samples were prepared by varying the thermal temperature and time. Those samples obtained at 200, 250, 350, 450 °C for 0.25 h were denoted as S200-1, S250-1, S350-1, and S450-1, respectively. The ones prepared at 200, 250, 350, 450 °C for 0.5 h were named as S200-2, S250-2, S350-2, and S450-2, respectively. In each case, all other experimental conditions were held constant.

The dendrite-shaped CuO hollow structures were characterized by field-emission scanning electron microscopy (FE-SEM; JEOL-JSM-6700F) operated at an acceleration voltage of 5 kV and high-resolution TEM (HR-TEM, JEOL JEM-2010FEF, 200 kV) for morphology and lattice images. The crystal structure of the sample was determined by X-ray powder diffraction (XRD) using Bruker D-8 Avance (Cu Kα irradiation, λ=1.54178 Å) at a scanning rate of 0.06°/s in 2θ ranging from 20° to 80°.

The working electrodes were prepared by casting a slurry consisting of 55 wt% active material (CuO powders), 25 wt% carbon black, and 20 wt% polyvinylidene fluoride (PVDF) onto a copper foil. Coin-type test cells were assembled by using working electrodes as the anode electrodes (relative to $LiCoO_2$ cathode electrode), Li foils as both the counter and reference electrodes, 1 M solution of $LiPF_6$ in ethylene carbonate (EC) and dimethyl carbonate (DMC) (1:1 by weight) as the electrolyte, and polypropylene foil (Celgard) as the separator. These cells were assembled in an argon-filled glovebox (Mbraun, Unilab, Germany) and cycled at different rates between voltage limits of 0.02 and 3 V. The cells were aged for 12 h before measurement. The charge–discharge cycling were carried out at room temperature (RT=25 °C) by using BTS Series (Neware Technology Limited Company).

3. Results and discussion

The XRD analysis shown in Fig. 1a confirms that the dendritic Cu precursors are pure face-centered cubic Cu metals (Joint Committee on Powder Diffraction Standards (JCPDS) No. 85-1326). Moreover, XRD was used to explain the components of our samples prepared at different temperatures for 0.5 h. As shown in Fig. 1b, with the increase of temperature from 200 to 450 °C, diffraction peaks for the monoclinic phase CuO (JCPDS No. 80-1917) appear and increase their intensity,

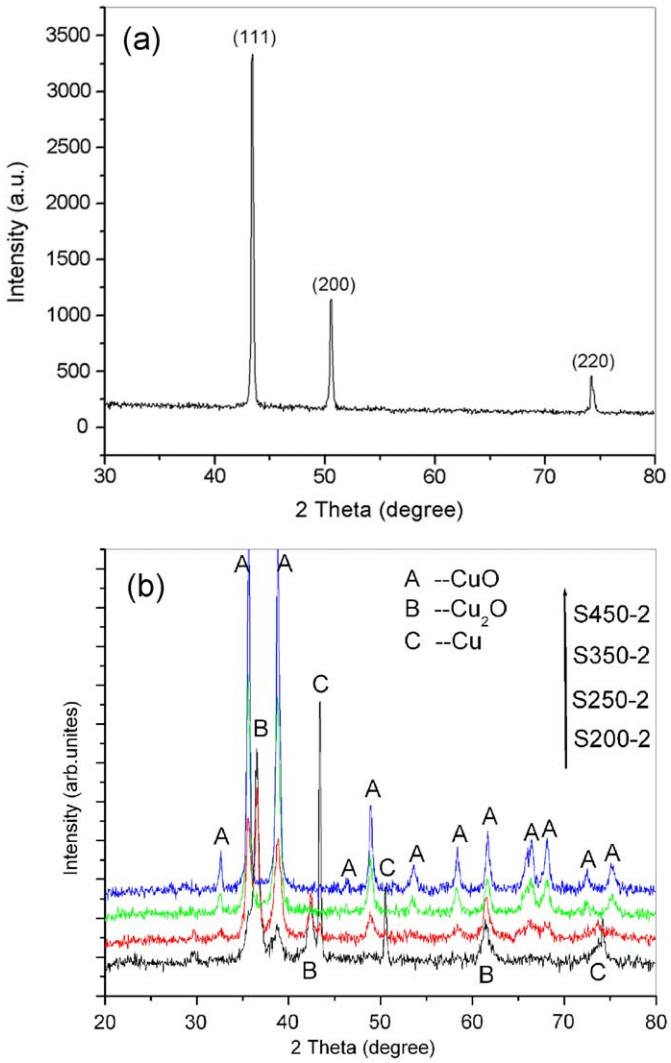

Fig. 1. The XRD patterns of (a) Cu precursors and (b) as-prepared products at 200–450 °C for 0.5 h.

while the cubic phase Cu (No. 85-1326) and cubic phase Cu_2O (No. 78-2076) peaks become weaker. The Bragg peaks of the products obtained at 200 and 250 °C are consistent with those of the Cu, Cu_2O and CuO phase. Instead, there is no hint of Cu and Cu_2O phase but all peaks of the samples can be indexed to the monoclinic phase CuO while the treatment temperature is up to 350 °C (see Fig. S1 in the Supporting Information). Therefore, the secondary growth temperature plays an important role in the crystal phase of the products.

Fig. 2a, b show the scanning electron microscopy (SEM) images of dendritic Cu precursors before further growth, and Fig. 2c, d show the morphology of the as-prepared CuO hollow architectures on heating primary Cu at 350 °C for 0.25 h. The Cu dendrites are 3–10 μm long and the diameter of the "branches" is approximately 160–170 nm. It can be seen that the CuO products have dendrite-shaped architectures, preserving their precursor morphology. The structural details are revealed in high-magnification SEM image (Fig. 2d). It can be observed that the internal diameter of the hollow branches is ~400 nm and the thickness of the tubes is ~350 nm. Fig. 2e displays a broken CuO dendrite, indicating that these dendrite-shaped CuO hollow structures are composed of cubic CuO nanoparticles outside and a dense film inside.

In order to confirm the hollow micro/nanostructure and discuss it in detail, we used transmission electron microscopy

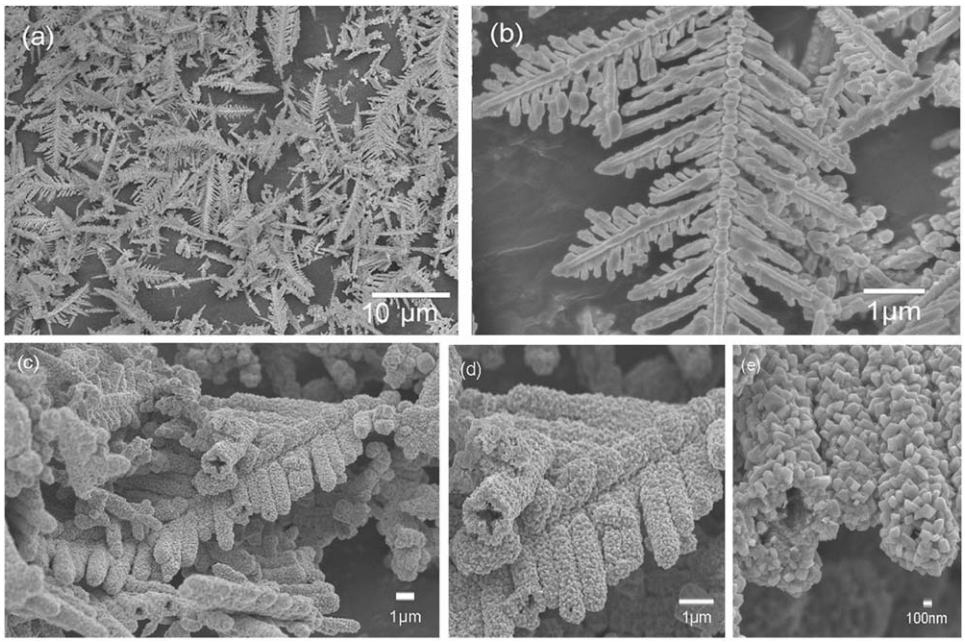

Fig. 2. FESEM images of Cu dendrites at (a) low magnification and (b) high magnification and typical CuO hollow strctures at (c) low magnification and (d, e) high magnification.

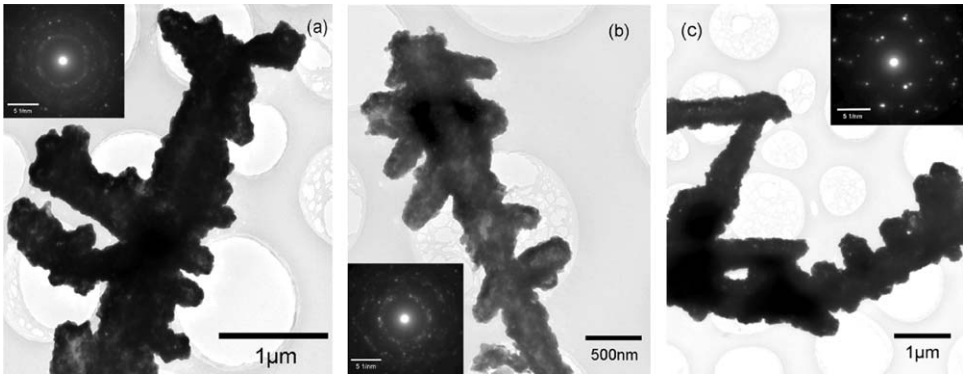

Fig. 3. TEM images of the products prepared at 350 °C for 5 min (a), 15 min (b), and 40 min (c).

(TEM) to investigate the samples prepared at 350 °C for 5, 15, 40 min in Fig. 3. TEM image of a dendrite-shaped Cu precursor is shown in Fig. S2. At first O_2 in the atmosphere can selectively nucleated at the external surfaces of the Cu dendrite, resulting in the formation of partial core–shell intermediate product (Fig. 3a). Subsequently, when the heating time is prolonged to 15 min, the hollow can be obtained obviously (Fig. 3b). Nevertheless, after thermal treatment in air for 40 min, CuO hollow structure becomes solid (Fig. 3c). Moreover, the selective area electronic diffraction (SAED) images (inset of Fig. 3) show that the crystallinity of the products increases with heating time. The sample obtained for 5 and 15 min is polycrystalline but the one attained for 40 min is monocrystalline.

A modified electroless deposition mechanism can be used to explain the growth of Cu dendrites [26]. In the initial stage of the growth process, Cu^{2+} ions combine with the Ac^- to form $Cu(Ac)_2$, a well-known rather weak electrolyte, in solution. Al metal loses electrons rapidly at first, according to the contrast of the cell potentials. Following this, Cu^{2+} ions released slowly from $Cu(Ac)_2$ accept the electrons donated by the Al foil and dendritic Cu nano- and microstructures generate. The release and diffusion of Cu^{2+} were too fast with the absence of HAc, and not beneficial to the nucleation and growth of dendritic Cu, which can be proved by our control experiments shown in Fig. S3.

Based on the features in the shape evolution process, the formation of dendrite-shaped CuO hollow structures is believed to be the results of Kirkendall effect, the basis of which is void formation caused by the difference in diffusion rates between two species [8,27]. The growth process for the hollow structures is schematically illustrated in Fig. 4. The formed Cu dendrites (a) are annealed in air at 250–450 °C, causing an interfacial solid-state reaction and non-equilibrium diffusion. The initial stage is O atoms in the air were adsorbed onto the surface of the dendritic precursors, and subsequent a combination reaction would occur in which the Cu is oxidized, and the copper diffuse outward to form a thin layer of CuO [28]. The Kirkendall effect involves disparate rates of transport for Cu and O atoms through the CuO barrier layer [29]. The net outward flow of copper core through the CuO shell led to the generation of small Kirkendall voids (b) [30]. The second stage is an increase of the gaps contributed by further surface diffusion of the core material along the pore surface (c). In this stage, voids began to develop and merge due to the high defect content and surface energy associated with the pore surface favor the nucleation of voids there. Finally, the

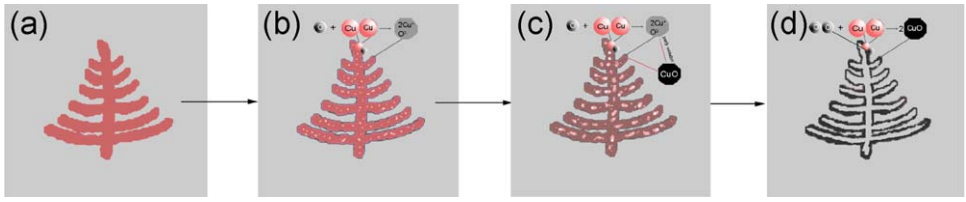

Fig. 4. Schematic illustration of the growth of typical dendrite-shaped CuO hollow architectures.

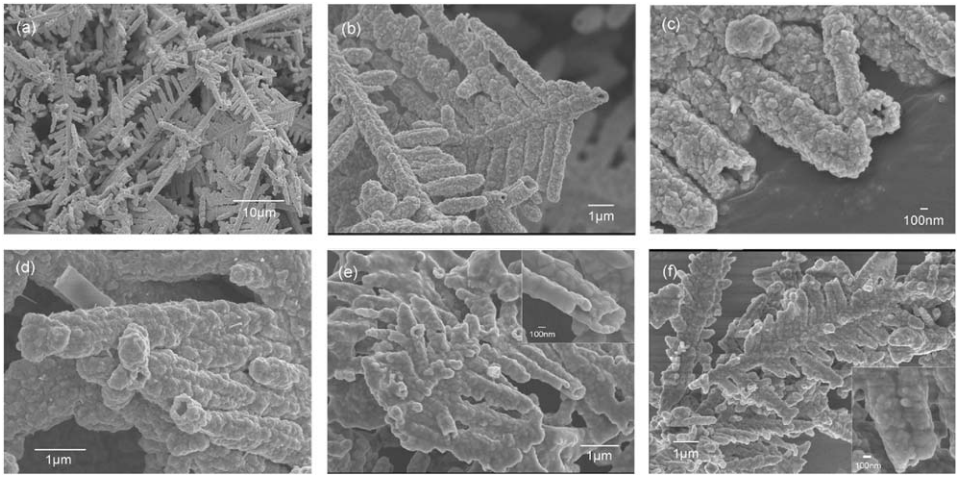

Fig. 5. FESEM images of the samples S250-1 (a, b), S250-2 (c), S350-2 (d), S450-1 (e), and S450-2 (f). The insets show the high-magnification pictures of the corresponding images.

material exchange can proceed thoroughly via gaps evaporation at high temperature. The existence of the CuO shell would condense to form hollow structures with similar morphology of the precursors (d) [30]. We speculate that after copper was oxidized completely, a similar sintering process happens. Voids would overflow time-dependently through diffusion induced by high temperature to cause the shrinkage and crystallization of the hollow. With the heating time increasing, the hollow structure could change into be solid and monocrystalline (Fig. 3c) [29].

To determine optimized reaction conditions for the best dendrite-shaped CuO hollow morphologies, various comparative experiments have been performed. Fig. 5 shows the FESEM images of S250-1, S250-2, S350-2, S450-1, and S450-2. The cube-like morphologies are barely discernible on the exterior surface of the hollow dendrites for the sample S250-1 (Fig. 5a, b). With increasing the reaction time to 0.5 h at 250 °C, these cube-like nanoparticles become distinctive (Fig. 5c), but the cubic nanostructures blurs with a further increase in the reaction temperature or time (Fig. 5d–f). These cubic nanoparticles are started to adhere and assemble each other at higher temperature and longer reaction time (inset of Fig. 5e, f). This is consistent with the results of TEM. Therefore, it can be inferred that 350 °C and 0.25 h are the best reaction temperature and time to obtain the best dendrite-shaped structures composed of well-defined cube nanoparticles outside and a dense film inside (Fig. 2e).

The CuO electrodes were examined with Li ion insertion and extraction to demonstrate their electrochemical performance in energy storage. The assembled cell was cycled between 0.02 and 3 V at room temperature. The electrochemical performance of the sample S350-1 electrode was investigated by galvanostatic discharge–charge measurements at a current rate of 0.5 C (C was defined as 2 Li^+ per hour; 670 mA h g^{-1}). As illustrated in Fig. 6a, the first discharge capacity is high, that is 1503.9 mA h g^{-1}, greater than the theoretical value. On the one hand, the extra capacity is attributed to the formation of a surface–electrolyte interphase (SEI) film due to electrolyte decomposition [31]. The low reversible capacity of carbon black contained in active materials, on the other hand, should not be neglected, because in our experiments, the active materials contain 25% carbon black, the first Coulombic efficiency of which is only about 26.7%. Fortunately, the contribution of carbon black towards the capacity of Li-ion battery becomes smaller and smaller along with the number of cycles increasing since the capacity of carbon black decreases very sharply during charge/discharge process [32]. Furthermore, we can observe a flat plateau near 1.05 V in the discharge curve, whereas there is only a subtle plateau near 2.5 V for Li release from the crystal lattice of CuO [20,33]. More details can be observed in the differential capacity plot (DCP, the inset of Fig. 6a). The peak at 0.35 V in the discharge curve can be ascribed to the formation of SEI. For conversion reactions of transition-metal oxides electrodes, the formation of SEI has been suggested upon discharge at low potentials [34]. Other peaks at 0.75 and 1.05 V in the discharge curve correspond to the multistep electrochemical Li reaction process or additional sites for Li uptake due to the formation of the imperfection of highly organized nanotextured CuO lattice with polycrystalline structure, which facilitates the transport of lithium in surface defects and in bulk materials [33]. In the charge curve, a peak centered at 2.5 V corresponds to a strong polarization [20,33]. From Fig. 6b, the second discharge and charge capacities are determined as 514.3 and 469.1 mA h g^{-1}, respectively. In addition, the CuO (S350-1) electrode is able to keep its discharge capacity at 481.7 mA h g^{-1} after 10 cycles and 437.4 mA h g^{-1} after 20 cycles, indicating a higher reversible capacity than traditional graphitic carbon. Fig. 6c shows the electrochemical response of sample S350-1 on cycling at a current

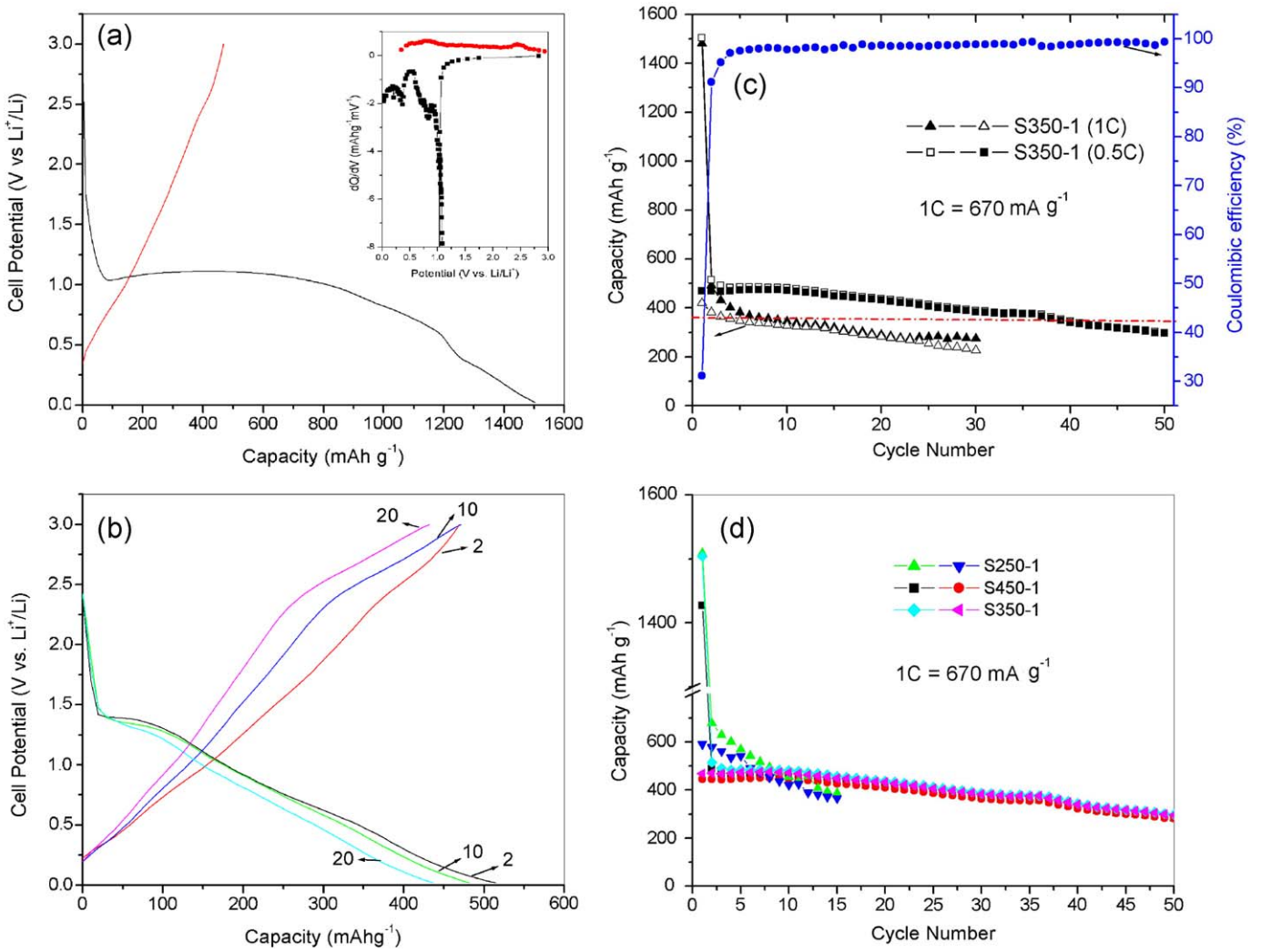

Fig. 6. (a) First and (b) 2nd, 10th, and 20th discharge/charge voltage profile of S350-1 cycled at a rate of 0.5 C. (c) Variation in discharge/charge capacity versus cycle number for S350-1 at different rates of 0.5 and 1 C. (d) Cycle life of the samples S250-1, S350-1, and S450-1 at a rate of 0.5 C. The inset shows the initial differential capacity plot of S350-1 at a rate of 0.5 C.

rate of 0.5 and 1 C at room temperature. The cell reveals the reversible capacity of $\sim$300 mA h g^{-1}, that is, 57.9% retention of the discharge capacity of the second cycle after 50 cycles. The average Coulombic efficiency of 50 cycles is up to $\sim$97.0%. At a rate of 1 C, the electrode is capable of delivering discharge capacity of 343.9 mA h g^{-1} after 10 cycles (close to graphite capacity: 372 mA h g^{-1}). The high capacity and good cyclability of the CuO electrodes mainly originate from their hollow structure consisted of nanocubes with structural robustness, such as alleviating the strains caused by the volume variation, short diffusion paths both for electrons and lithium ions as well as large electrode–electrolyte contact area [35,36].

Structure parameters of CuO hollow architectures are very crucial to the electrochemical behavior. To discuss the influence of CuO structure on the cell cycling performance, we show in Fig. 6d the cycling response of S250-1, S350-1, and S450-1 under the same conditions. The sample S350-1 reveals a better cycling performance than S250-1 and a higher capacity than S450-1. The discharge capacity of S250-1 rapidly declines to 386.3 mA h g^{-1} after 15 cycles, which is significantly poorer than that of S350-1. Both S450-1 and S350-1 show a decrease in discharge capacity with time. However, S350-1 displays a higher discharge capacity

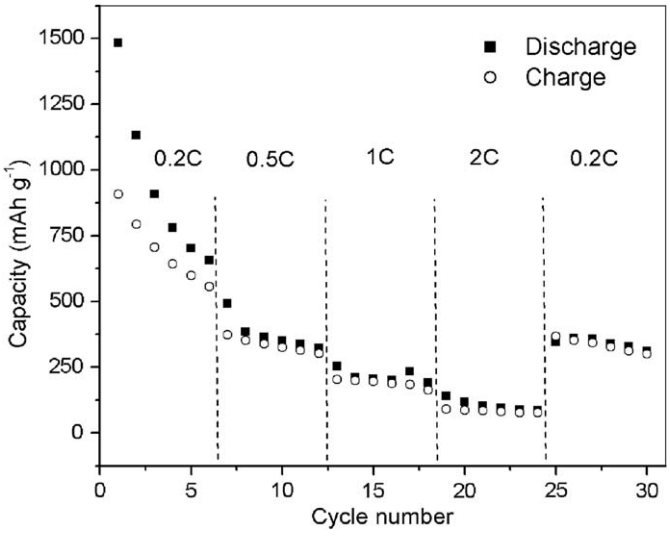

Fig. 7. Capacity delivered upon cycling at various rates by sample S350-1 cycled between 0.02 and 3 V.

than the sample S450-1. Therefore, from the previous characterization of the three samples, to achieve good performance, firstly, the primary particles that compose hollow dendrite-shaped structures should be as small as possible, that is, the Kirkendall effect should be sufficiently strong to minimize the constituent particles, leading to better contact between CuO and shorter diffusion length of lithium ions [25], which make an influence on the higher reversible capacity. Secondly, the hollow dendrites should have as large space as possible to accommodate the large volume change, delaying capacity fading [37,38]. The cycling response at progressively increasing rates of S350-1 shows in Fig. 7. At rate as high as 2C (1340 mA g^{-1}), the electrode reveals good cyclability and high Coulombic efficiency. By returning to the initial rate of 0.2 C, the reversible capacity is about 340 mA h g^{-1}, ~54% of the capacity at the 5th cycle.

We also point out that there are several additional advantages associated with the development of hollow nanostructured electrodes for Li-ion batteries. Those include, for example, fast electrolyte diffusion, higher electrode/electrolyte contact area leading to higher charge/discharge rates, and a structural buffer for the large volume expansion [39]. Problems still have to be overcome in terms of initial irreversible capacity. Further work on optimizing the surface morphology of electrode materials and using nanostructured current collectors to ensure better cycling performance is in progress.

4. Conclusion

In summary, dendrite-shaped CuO hollow micro/nanostructures can be produced in a Kirkendall-effect-based template-free thermal treatment process. The internal diameter of the hollow branches is ~400 nm and the as-prepared hollow structures are composed of nanocubes outside and a dense film inside. The crystalline structure and morphology of the products are highly dependent upon the treatment temperature and reaction time in the synthetic process. The fine and polycrystalline CuO hollow structures as anode materials for lithium-ion batteries exhibit a high initial discharge capacity of 1503.9 mA h g^{-1} with the average Coulombic efficiency of ~97.0% for the next 50 cycles over the potential range 0.02–3.0 V at a current rate of 0.5 C at room temperature. The electrochemical behavior lies crucially on the structural parameters of the CuO hollow architectures. The small primary particles that compose dendrite-shaped CuO and large space in the hollow structure are expected to improve the performance of the Li-ion cells. This Kirkendall-effect-based approach is proved to be an effective method to prepare excellent hollow electrode materials for Li-ion batteries.

Acknowledgment

The authors appreciate the financial support from the National Natural Science Foundation of China (Nos. 50872039 and 50802032).

Appendix A. Supplementary materials

Supplementary data associated with this article can be found in the online version at doi:10.1016/j.jssc.2010.01.013

References

[1] P. Jiang, J.F. Bertone, V.L. Colvin, Science 291 (2001) 453–457.
[2] F. Caruso, R.A. Caruso, H. Mohwald, Science 282 (1998) 1111–1114.
[3] F. Caruso, Adv. Mater. 13 (2001) 740–744.
[4] C.E. Fowler, D. Khushalani, S. Mann, J. Mater. Chem. 11 (2001) 1968–1971.
[5] H.W. Liang, S. Liu, J.Y. Gong, S.B. Wang, L. Wang, S.H. Yu, Adv. Mater. 21 (2009) 1850–1854.
[6] F. Tao, C. Gao, Z. Wen, Q. Wang, J. Li, Z. Xu, J. Solid State Chem. 182 (2009) 1055–1060.
[7] J. Liu, D. Xue, Adv. Mater. 20 (2008) 2622–2627.
[8] H.J. Fan, U. Gösele, M. Zacharias, Small 3 (2007) 1660–1671.
[9] M.F. Luo, Y.P. Song, J.Q. Lu, X.Y. Wang, Z.Y. Pu, J. Phys. Chem. C 111 (2007) 12686–12692.
[10] J. Chen, K. Wang, L. Hartman, W. Zhou, J. Phys. Chem. C 112 (2008) 16017–16021.
[11] J.H. Schon, M. Dorget, F.C. Beuran, X.Z. Zu, E. Arushanov, C.D. Cavellin, M. Lagues, Nature 414 (2001) 434–436.
[12] L. Liao, Z. Zhang, B. Yan, Z. Zheng, Q.L. Bao, T. Wu, C.M. Li, Z.X. Shen, J.X. Zhang, H. Gong, J.C. Li, T. Yu, Nanotechnology 20 (2009) 085203–085208.
[13] Y. Chang, H.C. Zeng, Cryst. Growth Des. 4 (2004) 397–402.
[14] Y.W. Zhu, T. Yu, F.C. Cheong, X.J. Xu, C.T. Lim, V.B.C. Tan, J.T.L. Thong, C.H. Sow, Nanotechnology 16 (2005) 88–92.
[15] S. Wang, H. Xu, L. Qian, X. Jia, J. Wang, Y. Liu, W. Tang, J. Solid State Chem. 182 (2009) 1088–1093.
[16] J. Liu, X. Huang, Y. Li, K.M. Sulieman, X. He, F. Sun, Cryst. Growth Des. 6 (2006) 1690–1696.
[17] S. Gao, S. Yang, J. Shu, S. Zhang, Z. Li, K. Jiang, J. Phys. Chem. C 112 (2008) 19324–19328.
[18] P. Poizot, S. Laruelle, S. Grugeon, L. Dupont, J.M. Tarascon, Nature 407 (2000) 496–499.
[19] Y.S. Hu, Y.G. Guo, W. Sigle, S. Hore, P. Balaya, J. Maier, Nat. Mater. 5 (2006) 713–717.
[20] J. Morales, L. Sanchez, F. Martin, J.R. Ramos-Barrado, M. Sanchez, Electrochim. Acta 49 (2004) 4589–4597.
[21] Q. Pan, H. Jin, H. Wang, G. Yin, Electrochim. Acta 53 (2007) 951–956.
[22] S.F. Zheng, J.S. Hu, L.S. Zhong, W.G. Song, L.J. Wan, Y.G. Guo, Chem. Mater. 20 (2008) 3617–3622.
[23] F.S. Ke, L. Huang, G.Z. Wei, L.J. Xue, J.T. Li, B. Zhang, S.R. Chen, X.Y. Fan, S.G. Sun, Electrochim. Acta 54 (2009) 5825–5829.
[24] L.B. Chen, N. Lu, C.M. Xu, H.C. Yu, T.H. Wang, Electrochim. Acta 54 (2009) 4198–4201.
[25] J.Y. Xiang, J.P. Tu, L. Zhang, Y. Zhou, X.L. Wang, S.J. Shi, J. Power Sources 195 (2010) 313–319.
[26] C. Yan, D. Xue, Cryst. Growth Des. 8 (2008) 1849–1854.
[27] Y. Yin, R.M. Rioux, C.K. Erdonmez, S. Hughes, G.A. Somorjai, A.P. Alivisatos, Science 304 (2004) 711–714.
[28] C.H.B. Ng, H. Tan, W.Y. Fan, Langmuir 22 (2006) 9712–9717.
[29] Q. Wang, J.X. Li, G.D. Li, X.J. Cao, K.J. Wang, J.S. Chen, J. Crystal Growth 299 (2007) 386–392.
[30] Y. Yin, R.M. Rioux, C.K. Erdonmez, S. Hughes, G.A. Somorjai, A.P. Alivisatos, Science 304 (2004) 711–714.
[31] D. Deng, J.Y. Lee, Chem. Mater. 20 (2008) 1841–1846.
[32] G. Li, R. Xue, L. Chen, Y.Z. Huang, J. Power Sources 54 (1995) 271–275.
[33] X.P. Gao, J.L. Bao, G.L. Pan, H.Y. Zhu, P.X. Huang, F. Wu, D.Y. Song, J. Phys. Chem. B 108 (2004) 5547–5551.
[34] D. Aurbach, A. Zaban, Y. Ein-Ein, I. Weissman, O. Chusid, B. Markovsky, M. Levi, E. Levi, A. Schechter, E. Granot, J. Power Sources 68 (1997) 91–98.
[35] C.J. Curtis, J. Wang, D.L. Schulz, J. Electrochem. Soc. 151 (2004) A590–A598.
[36] H.Y. Wang, T. Abe, S.H. Maruyama, Y. Iriyama, Z. Ogumi, K. Yoshikawa, Adv. Mater. 17 (2005) 2857–2860.
[37] X.W. Lou, L.A. Archer, Z.C. Yang, Adv. Mater. 20 (2008) 3987–4019.
[38] K.T. Lee, Y.S. Jung, S.M. Oh, J. Am. Chem. Soc. 125 (2003) 5652–5653.
[39] A.S. Arico, P. Bruce, B. Scrosati, J.M. Tarascon, W.V. Schalkwijk, Nat. Mater. 4 (2005) 366–377.